Theor Chem Acc (2000) 104:7–12
DOI 10.1007/s002149900094

Theoretical
Chemistry Accounts

*Regular article*

# Ab initio study on the dynamical properties of the hydrogen abstraction reaction $NH_2 + OH \rightarrow NH + H_2O$

**Zhen-Feng Xu**[1,2], **De-Cai Fang**[1], **Xiao-Yuan Fu**[1]

[1] Department of Chemistry, Beijing Normal University, Beijing 100875, China
[2] Department of Applied Chemistry, Beijing University of Chemical Technology, Beijing 100029, China

Received: 23 April 1999 / Accepted: 9 June 1999 / Published online: 15 December 1999


**Abstract.** The geometry of the transition state of the title reaction was optimized at the unrestricted Hartree–Fock, the spin-unrestricted second-order Møller–Plesset, and the spin-unrestricted quadratic configuration interaction with all single and double substitutions levels of theory. The changes in the geometry, the bound vibrational modes, and the potential energy along the minimum energy path are discussed. Variational transition-state theory rate constants calculated with the tunneling and curvature effect correction agree very well with the experimental values.

**Key words:** Hydrogen abstraction – Dynamic property – Ab initio MO

## 1 Introduction

The reactions of the amidogen radical, $NH_2(X^2B_1)$, with other radicals are important for understanding the thermal De-$NO_x$ process [1], in which NO that is formed during combustion is converted into molecular nitrogen. One of these reactions, $NH_2 + OH \rightarrow NH + H_2O$, is considered to be a kinetically sensitive reaction in the thermal De-$NO_x$ process. In 1982, Dean et al. [2] used a rate constant expression, $3.0 \times 10^{10} T^{0.68} \exp(-1200/RT)$ $cm^3\ mol^{-1}\ s^{-1}$, in the mechanism of ammonia oxidation over the temperature range from 1279 to 1323 K. In 1989, Miller and Bowman [1] used another rate constant expression, $4.0 \times 10^6 T^2 \exp(-1000/RT)$ $cm^3\ mol^{-1}\ s^{-1}$, to investigate the thermal De-$NO_x$ mechanism in the temperature range 1150–1350 K. From both the rate constant expressions, we can see that their activation energies are very close, while their rate constants are not consistent with each other. To our knowledge, the dynamical properties of this reaction have not been studied theoretically; therefore, we decided to study this reaction by using quantum chemistry and chemical reaction dynamics.

Dynamical calculations based on variational transition-state theory (VTST) constitute a practical methodol for studying polyatomic reactions [3–6]. Such calculations describe a chemical reaction by using ab initio electronic structure information only in the region of configuration space along the reaction path.

In the present paper, we use ab initio molecular orbital theory and the VTST dynamical method for the hydrogen abstraction reaction $NH_2 + OH \rightarrow NH + H_2O$. The second section of this paper describes the theoretical methods and computational details. In the third section, the stationary points on the hydrogen abstraction reaction path are optimized, and the minimum energy path (MEP) is calculated along the intrinsic reaction coordinate. The information about the potential energy, geometric variations, and generalized normal mode vibrational frequencies along the reaction path is also discussed. At the end of the third section, the rate constants based on conventional TST and, on VTST are presented and compared with the experimental values.

## 2 Computational methods

In this work, ab initio molecular orbital calculations were carried out with the GAUSSIAN 92 program [7] for the stationary points on the reaction path of the title reaction. The geometries of the reactants ($NH_2$ and OH), products (NH and $H_2O$), and transition states were optimized by using unrestricted Hartree–Fock (UHF) theory [8], spin-unrestricted Møller–Plesset perturbation (UMP) theory [9], and spin-unrestricted quadratic configuration interaction with all single and double substitutions (UQCISD) theory [10], respectively. The Møller–Plesset perturbation (UMP2) calculations include full electron correlation, while in the fourth-order Møller–Plesset perturbation (UMP4) and UQCISD calculations the frozen-core approximation has been employed. Furthermore, we used the scaling all correlation (SAC) method [11] in the UMP4/6-311G** calculation at the UMP2/6-311G** optimized geometries to yield an improved calculation of the barrier height. For the UMP-SAC4//MP2 calculation, the total electronic energy is [11]

$$E_{\mathrm{MP-SAC4//MP2}} = E_{\mathrm{HF}} + (E_{\mathrm{MP4}} - E_{\mathrm{HF}})/f_4 \ ,$$

*Correspondence to:* X.-Y. Fu

where $f_4$ is a scaling factor which is assumed to be independent of the geometry for a given system.

The MEP was calculated at the UMP2/6-311G** level of theory using intrinsic reaction coordinate theory [12–14] with a stepsize of 0.02 $(amu)^{1/2}$bohr. At some points along the intrinsic reaction coordinate, we computed the matrix of force constants and the harmonic vibrational frequencies. Because the shape of the potential-energy curve is an important factor affecting the rate constant, the UMP2 potential profile was refined at the UQCISD(T) and UMP-SAC4 levels with the same basis set.

The canonical VTST rate constant, $k^{CVT}(T)$, was calculated at a fixed temperature ($T$) by minimizing the generalized TST rate constant, $k^{GT}(T,s)$, with respect to the dividing surface at $s$. The result is expressed as [3–6]

$$k^{CVT}(T) = \min_s k^{GT}(T,s) \ .$$

The generalized TST rate constant, $k^{GT}$, for temperature $T$ and dividing surface at $s$ is

$$K^{GT}(T,s) = \frac{\sigma Q^{GT}(T,s)}{\beta h Q^{R}(T)} \exp[-\beta V_{MEP}(s)] \ .$$

In this equation, $s$ is the location of the generalized transition state on the MEP; $\sigma$ is the symmetry factor accounting for the possibility of two or more symmetry-related reaction paths; $\beta$ equals $(k_B T)^{-1}$, where $k_B$ is Boltzmann's constant, $h$ is Planck's constant; $Q^R(T)$ is the reactant's partition function per unit volume, excluding symmetry numbers for rotation; $V_{MEP}(s)$ is the classical energy along the MEP with the overall zero of energy at the reactant; $Q^{GT}(T,s)$ is the partition function of the generalized transition state at $s$ with the local zero of energy at $V_{MEP}(s)$ and with all rotational symmetry numbers set to unity. For $s = 0$, this equation yields the conventional TST rate constant ($k^{TST}$). To include quantal effects for motion along the reaction coordinate, $k^{CVT}(T)$ is multiplied by a ground-state transmission coefficient, $\kappa^{CVT/G}(T)$ with the zero-curvature tunneling (ZCT) and small-curvature tunneling (SCT) approximations [5,15], which are denoted as $k^{CVT/ZCT}(T)$ and $k^{CVT/SCT}(T)$, respectively. The POLYRATE program [16] was employed for the calculations of the reaction rate constants.

## 3 Results and discussion

The optimized geometrical parameters and harmonic frequencies of the reactants ($NH_2$ and OH) and products (NH and $H_2O$) are listed in Table 1. It can be seen that at the UHF level the bond lengths are slightly shorter and the bond angles are slightly greater than the experimental ones. When electronic correlation correction is introduced, the optimized geometries agree better with the experimental values. At the UMP2 level the deviations between the calculated and the experimental vibrational frequencies are mostly less than 9%, while at the UHF level the deviations are mostly greater than 9%, except for the OH and NH radicals. This provides confidence in the UMP2 level for studying this reaction process.

The geometric parameters and harmonic frequencies of the transition state optimized at various levels are displayed in Table 2. The transition state is a triplet state and $\langle S^2 \rangle = 2.038$. The imaginary vibrational mode and the atom-numbering system of the transition state are shown in Fig. 1. At the UHF/6-311G** level, the breaking $N_{(1)}$—$H_{(3)}$ bond of the transition state is stretched by about 16% compared to that in $NH_2$, while the forming $H_{(3)}$—$O_{(4)}$ bond is still 34% longer than that of $H_2O$. At the UMP2/6-311G** level, the breaking $N_{(1)}$—$H_{(3)}$ bond is stretched by about 7% compared to that in $NH_2$, and the forming $H_{(3)}$—$O_{(4)}$ bond length is 44% longer than that in $H_2O$. It is obvious that the transition state structure is more reactant-like than productlike. On the other hand, the breaking $N_{(1)}$—$H_{(3)}$ bond and the forming $H_{(3)}$—$O_{(4)}$ bond of the transition state at the UMP2 level are slightly shorter and longer than those at the UHF level, respectively. Also, the geometric parameters of the transition state optimized at the UQCISD/6-311G** level of theory are almost consistent with those optimized at the UMP2 level of theory. This shows that the geometry of the transition state of this reaction optimized at the UMP2/6-311G** level of theory is quite reliable. Comparing the frequencies at the UMP2 level with those at the UHF level, we find that the imaginary frequency at the former level is about 2100 $cm^{-1}$ less than that at the latter level, while there are smaller variations in the real frequencies.

In order to illustrate the applicability of an UHF single-configuration reference state, a multiconfiguration self-consistent-field calculation was carried out for the transition state at the UMP2/6-311G** geometry. A complete active space involving six electrons and six orbitals with the 6-311G** basis set was performed. The result shows that the coefficient of the ground-state

**Table 1.** Optimized geometric parameters (Å and degree) and harmonic frequencies ($cm^{-1}$) of reactants and products

| | $NH_2$ | | OH | NH | $H_2O$ | | $NH_2$ | | | OH | NH | $H_2O$ | | |
|---|---|---|---|---|---|---|---|---|---|---|---|---|---|---|
| | $R_{N\text{-}H}$ | $\theta_{H\text{-}N\text{-}H}$ | $R_{O\text{-}H}$ | $R_{N\text{-}H}$ | $R_{O\text{-}H}$ | $\theta_{H\text{-}O\text{-}H}$ | $\omega(a_1)$ | $\omega(a_1)$ | $\omega(b_1)$ | $\omega(\sigma)$ | $\omega(\sigma)$ | $\omega(a_1)$ | $\omega(a_1)$ | $\omega(b_1)$ |
| UHF/6-31G | 1.015 | 108.5 | 0.967 | 1.032 | 0.950 | 111.5 | 1651 | 3552 | 3647 | 3831 | 3372 | 1736 | 3988 | 4145 |
| UHF/6-31G* | 1.013 | 104.4 | 0.958 | 1.024 | 0.947 | 105.5 | 1711 | 3607 | 3707 | 4003 | 3529 | 1826 | 4070 | 4188 |
| UHF/6-31G** | 1.013 | 104.3 | 0.955 | 1.024 | 0.943 | 105.9 | 1656 | 3609 | 3706 | 4056 | 3514 | 1770 | 4145 | 4262 |
| UHF/6-311G** | 1.012 | 104.1 | 0.951 | 1.023 | 0.941 | 105.4 | 1643 | 3599 | 3683 | 4053 | 3501 | 1751 | 4141 | 4236 |
| UMP2/6-31G* | 1.028 | 103.4 | 0.979 | 1.039 | 0.968 | 104.0 | 1632 | 3423 | 3545 | 3740 | 3366 | 1735 | 3778 | 3920 |
| UMP2/6-31G** | 1.023 | 102.6 | 0.971 | 1.035 | 0.961 | 103.8 | 1596 | 3484 | 3599 | 3844 | 3407 | 1684 | 3893 | 4031 |
| UMP2/6-311G** | 1.024 | 102.1 | 0.966 | 1.035 | 0.957 | 102.5 | 1545 | 3459 | 3560 | 3860 | 3392 | 1667 | 3910 | 4017 |
| UQCISD/6-311G** | 1.029 | 101.8 | 0.969 | 1.042 | 0.957 | 102.7 | 1578 | 3416 | 3514 | 3833 | 3331 | 1722 | 3914 | 4030 |
| Experimental[a] | 1.024 | 103.3 | 0.971 | 1.035 | 0.958 | 104.5 | 1497[b] | 3219 | 3301 | 3735[c] | 3282[c] | 1588[d] | 3650 | 3742 |

[a] Ref. [17]
[b] Ref. [18]
[c] Ref. [19]
[d] Ref. [20]

**Table 2.** Optimized geometric parameters and harmonic frequencies of the transition state

| | Geometry parameters (Å and degree) | | | | | | | | |
|---|---|---|---|---|---|---|---|---|---|
| | $R_{12}$ | $R_{13}$ | $R_{34}$ | $R_{45}$ | $\theta_{312}$ | $\theta_{431}$ | $\theta_{543}$ | $\varphi_{4312}$ | $\varphi_{5431}$ |
| UHF/6-31G | 1.023 | 1.190 | 1.276 | 0.964 | 102.5 | 174.2 | 101.2 | 1.1 | 178.6 |
| UHF/6-31G* | 1.018 | 1.186 | 1.259 | 0.956 | 100.0 | 168.9 | 97.9 | 48.4 | 99.0 |
| UHF/6-31G** | 1.018 | 1.174 | 1.260 | 0.953 | 99.9 | 169.0 | 97.6 | 46.1 | 99.9 |
| UHF/6-311G** | 1.016 | 1.174 | 1.262 | 0.949 | 101.0 | 162.6 | 96.2 | 29.8 | 80.4 |
| UMP2/6-31G* | 1.030 | 1.111 | 1.372 | 0.979 | 104.0 | 146.9 | 99.9 | 9.3 | 73.0 |
| UMP2/6-31G** | 1.026 | 1.095 | 1.384 | 0.972 | 103.6 | 148.0 | 99.8 | 9.2 | 68.2 |
| UMP2/6-311G** | 1.027 | 1.093 | 1.386 | 0.967 | 102.7 | 150.2 | 98.5 | 9.1 | 67.8 |
| UQCISD/6-311G** | 1.031 | 1.104 | 1.384 | 0.968 | 103.4 | 149.6 | 98.4 | 6.7 | 69.2 |
| | Frequencies ($cm^{-1}$) | | | | | | | | |
| | $\omega_1$ | $\omega_2$ | $\omega_3$ | $\omega_4$ | $\omega_5$ | $\omega_6$ | $\omega_7$ | $\omega_8$ | $\omega_F$ |
| UHF/6-31G | 3875 | 3514 | 1563 | 1043 | 740 | 556 | 389 | 48 | *i*3801 |
| UHF/6-31G* | 4022 | 3612 | 1546 | 1161 | 762 | 510 | 424 | 66 | *i*3790 |
| UHF/6-31G** | 4083 | 3610 | 1506 | 1136 | 782 | 522 | 433 | 33 | *i*3722 |
| UHF/6-311G** | 4078 | 3598 | 1429 | 1298 | 797 | 548 | 441 | 77 | *i*3687 |
| UMP2/6-31G* | 3730 | 3473 | 1770 | 1209 | 1087 | 693 | 402 | 345 | *i*1949 |
| UMP2/6-31G** | 3834 | 3525 | 1825 | 1155 | 1092 | 600 | 371 | 200 | *i*1640 |
| UMP2/6-311G** | 3847 | 3492 | 1777 | 1144 | 1056 | 586 | 378 | 192 | *i*1514 |

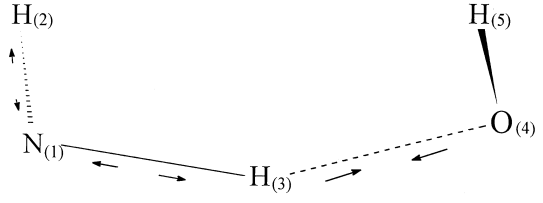


**Fig. 1.** Structure and imaginary vibrational mode of the transition state

configuration is 0.982 and the absolute magnitudes of the coefficients of other configurations are all less than about 0.088. Thus, the single dominant determinant can afford a sufficiently accurate reference of this reaction.

The potential-energy barrier ($V^*$) and the heat of reaction ($\Delta H$) at each level of theory are listed in Table 3. The absolute values of $\Delta H$ at the UMP2 levels are about 9 kcal/mol greater than those at the UHF levels. The heats of reaction obtained by single-point energy calculations at the UMP4, UQCISD(T), and UMP-SAC4 levels based on the UMP2/6-311G** geometries are −25.94, −25.42, and −27.34 kcal/mol, respectively. The heat of reaction at the UMP-SAC4 level is in good agreement with the experimental value. From Table 3, we can see that there are significant differences in the potential barrier height for the different basis sets and different levels of calculations. At the UHF level the potential barrier height is apparently overestimated, while at the UMP2 and UQCISD levels it is still much greater than the experimental ones. Accurate theoretical potential energy barriers are calculated at the UMP4, UQCISD(T), and UMP-SAC4 levels at the UMP2/6-311G** geometries. Apparently, the value of the UQCISD(T) barrier is slightly greater than the value of Dean et al. [2], and the value of the UMP-SAC4 barrier is slightly less than that of Miller and Bowman [1].

The MEP was calculated with a step size of 0.02 $(amu)^{1/2}$bohr at the UMP2/6-311G** level. Then the UMP2/6-311G** potential-energy profile was further refined with the UQCISD(T) and UMP-SAC4 levels. The minimum-potential-energy curve, $V_{MEP}(s)$, and the corresponding vibrationally adiabatic ground-state potential-energy curve, $V_a^G(s)$, based on the UMP-SAC4 method, are shown in Fig. 2. The main geometrical changes along the MEP are shown in Fig. 3. It appears that the $H_{(3)}$—$O_{(4)}$ distance shortens linearly along $s$ and reaches the bond length of $H_2O$ at about $s = 0.8$ $(amu)^{1/2}$bohr, while the $N_{(1)}$—$H_{(3)}$ bond length starts elongating at about $s = -0.2$ $(amu)^{1/2}$bohr and tends linearly to infinity. Both the $N_{(1)}$—$H_{(2)}$ and the $O_{(4)}$—$H_{(5)}$ bond lengths do not vary during the reaction process. It is thus evident that the hydrogen abstraction from $N_{(1)}$ to $O_{(4)}$ essentially takes place in the region of $s = -0.2$–$0.8$ $(amu)^{1/2}$bohr.

The frequency changes of the eight bound vibrational modes calculated at the UMP2/6-311G** level are shown in Fig. 4. At the beginning of the reaction, there exists the stretching vibrational mode of OH, which is related to mode 1, and the three vibrational modes of $NH_2$, which are related to modes 4, 3, and 2. At the end of the reaction, three vibrational modes of $H_2O$ are associated with modes 5, 3, and 1, and the NH stretching vibration is associated with mode 2. Modes 6, 7, and 8 appear only near the transition state and the their frequencies are smaller. The frequency of mode 5 increases significantly as the reaction proceeds and reaches the symmetric bending vibrational frequency of $H_2O$ at about $s = 0.6$ $(amu)^{1/2}$bohr, while the frequency of mode 4, relating to the symmetric bending vibration of $NH_2$, decreases rapidly after the transition state and tends to zero. The frequencies of modes 1 and 2 have no obvious variations during the course of the reaction; however, we can easily find that the change in frequency of mode 3 is the most noticeable one. It starts from the symmetric stretching vibrational frequency of the $NH_2$ radical, drops rapidly after about $s = -0.5$ $(amu)^{1/2}$bohr, and reaches the minimum (about 1500 $cm^{-1}$) at about

**Table 3.** Potential energy barrier ($V^{\neq}$) with zero-point vibrational energy correction ($ZPE$) and heat of reaction ($\Delta H^0_{298}$) in kilocalories per mole

| | Forward reaction | | Reverse reaction | | $\Delta H^0_{298}$ |
|---|---|---|---|---|---|
| | $V_f^{\neq}$ | $V_f^{\neq}+\Delta$ZPE | $V_r^{\neq}$ | $V_r^{\neq}+\Delta$ZPE | |
| Optimized | | | | | |
| UHF/6-31G | 18.42 | 16.76 | 38.52 | 36.36 | −19.32 |
| UHF/6-31G* | 21.09 | 19.78 | 40.04 | 37.88 | −18.09 |
| UHF/6-31G** | 19.92 | 18.44 | 40.7 | 38.28 | −19.80 |
| UHF/6-311G** | 19.73 | 18.72 | 40.69 | 38.74 | −20.02 |
| UMP2/6-31G* | 7.48 | 8.01 | 34.44 | 33.52 | −26.76 |
| UMP2/6-31G** | 5.22 | 5.48 | 33.85 | 33.42 | −27.94 |
| UMP2/6-311G** | 4.59 | 4.67 | 33.91 | 33.26 | −28.51 |
| UQCISD/6-311G** | 2.82 | | 28.78 | | −25.02 |
| Single-point energy calculations at the UMP2/6-311G** geometry | | | | | |
| UMP4/6-311G** | 3.65 | 3.76 | 30.4 | 29.78 | −25.94 |
| UQCISD(T)/6-311G** | 1.43 | 1.54 | 27.66 | 27.04 | −25.42 |
| UMP-SAC4 | 0.69 | 0.80 | 28.84 | 28.22 | −27.34 |
| Experimental | 1.00[a]<br>1.20[b] | | | | −28.2[c] |

[a] Ref. [1]
[b] Ref. [2]
[c] The heat of reaction was obtained from the experimental heats of formation of the reactants ($NH_2$ and OH) and products (NH and $H_2O$), which are taken from Ref. [21]

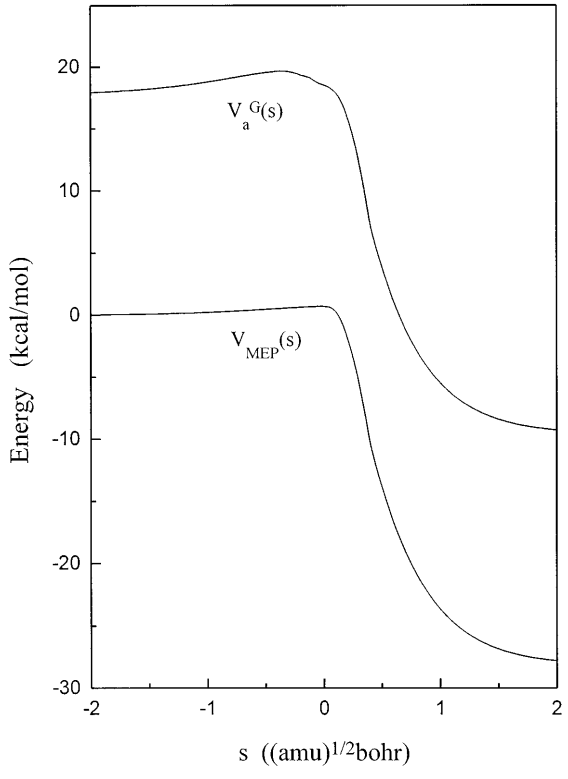


**Fig. 2.** Minimum energy path, $V_{MEP}(s)$, and vibrationally adiabatic ground-state potential-energy curve, $V_a^G$ ($s$) at the UMP-SAC4 level of theory

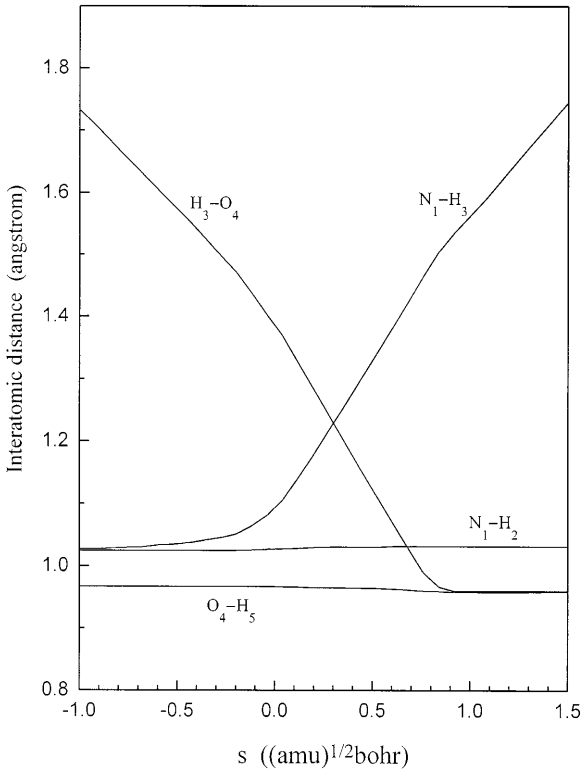


**Fig. 3.** Changes in interatomic distances calculated at the UMP2/6-311G** level of theory

$s$ = 0.2 (amu)$^{1/2}$bohr. Then, at about $s$ = 0.5 (amu)$^{1/2}$ bohr it rapidly increases and reaches the symmetric stretching vibrational frequency of $H_2O$ at about $s$ = 1.0 (amu)$^{1/2}$bohr. Namely, mode 3 represents mainly the hydrogen atom abstraction process. In the course of the frequency change of mode 3 there is a minimum of about 1800 cm$^{-1}$ and the dip occurs over $s$ = −0.5–0.8 (amu)$^{1/2}$bohr. This means that the hydrogen abstraction reaction happens substantially in the narrow region from $s$ = −0.5 to $s$ = 0.8 (amu)$^{1/2}$bohr. In this region, the concerted transforming process of the hydrogen atom $H_{(3)}$ from the stretching vibration of the old bond $N_{(1)}$—$H_{(3)}$ to the stretching vibration of the new bond $O_{(4)}$—$H_{(3)}$ takes place. This region is approximately the same as where the main change in geometry depicted in Fig. 3 occurs; therefore, mode 3 can be referred to as the "reactive mode" in the hydrogen abstraction reaction. The coupling constants between the MEP and the vibrational modes orthogonal to the MEP show that there is a strong coupling between

the MEP and mode 3 in the reactant side of the transition state. The effective energy exchange between mode 3 and the MEP would favor the hydrogen abstraction reaction of OH from $NH_2$.

The reaction rate constants for the temperature range from 400 to 3000 K, which are calculated by conventional TST and by VTST with the ZCT and SCT contributions at the UMP2, UQCISD(T), and UMP-SAC4 levels of theory are listed in Table 4. Arrhenius plots of the UMP-SAC4, UMP2, and experimental rate constants are shown in Fig. 5. It is found the reaction rate constants calculated at the UQCISD(T) and UMP-SAC4 levels are in good agreement with the values of Miller and Bowmann over the temperature range 700–3000 K and with the values of Dean et al. over the temperature range 400–800 K, while those at the UMP2 level deviate significantly from the experimental result.

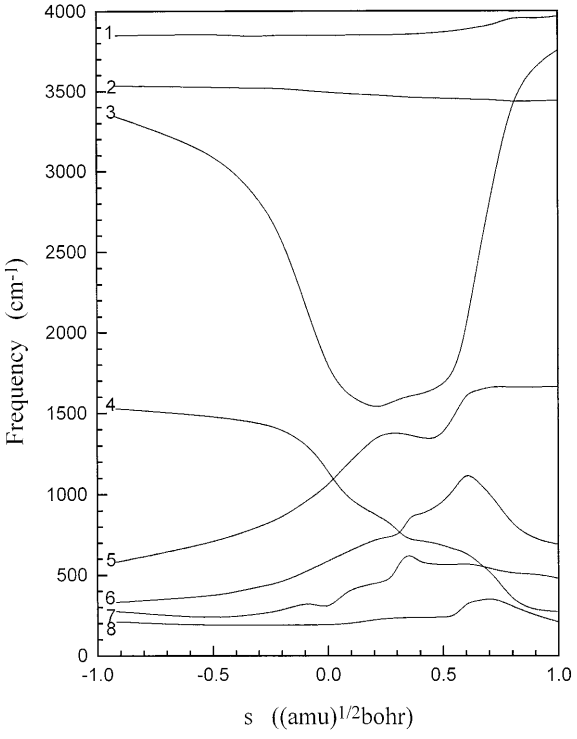


**Fig. 4.** Changes in vibrational frequencies calculated at the UMP2/6-311G** level of theory

By comparing the results of VTST with conventional TST, one finds that over all the temperature range the variational effect makes the rate constant decrease by about 20%. The locations of the variational transition state are $s = -0.128$, $-0.111$, 0.008, and 0.121 $(\text{amu})^{1/2}$

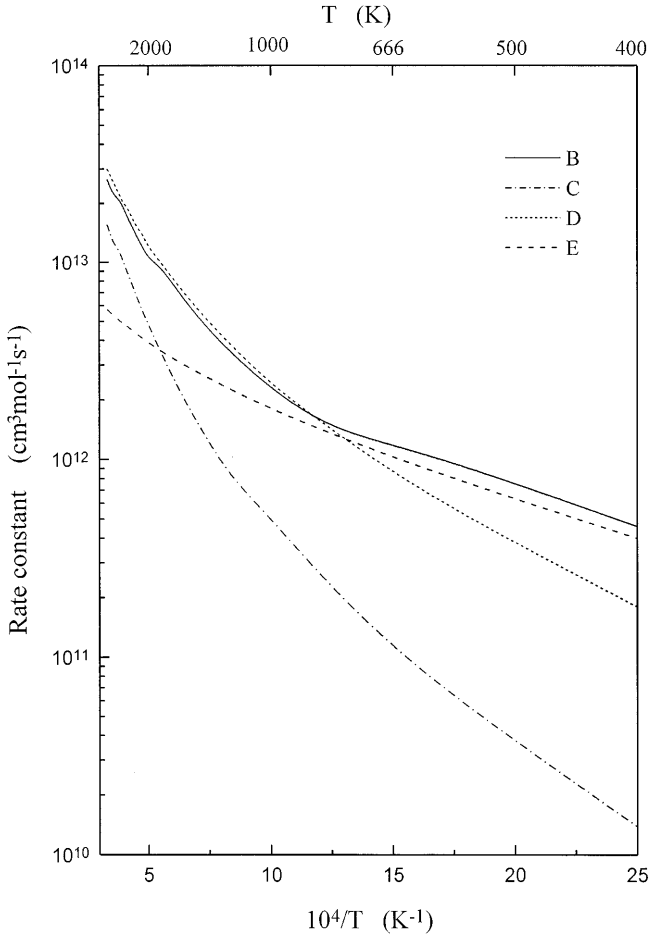


**Fig. 5.** Arrhenius plot of the theoretical and experimental rate constants versus reciprocal temperature. *B* Canonical variational transition-state theory (*CVT*)/small-curvature tunneling (*SCT*) rate constant at UMP-SAC4; *C* CVT/SCT rate constant at UMP2/6-311G**; *D* rate constant expression of Miller and Bowmann [1], $4.0 \times 10^6 T^2 \exp(-1000/RT)$ cm$^3$ mol$^{-1}$ s$^{-1}$; *E* rate constant expression of Dean et al. [2], $3.00 \times 10^{10} T^{0.68} \exp(-1200/RT)$ cm$^3$ mol$^{-1}$ s$^{-1}$

**Table 4.** Reaction rate constants (cm$^3$ mol$^{-1}$ s$^{-1}$) over the temperature range 400–3000 K

| *T* (K) | UMP2 | | | | UQCISD(T)//UMP2 | | | | UMP-SAC4//UMP2 | | | |
|---|---|---|---|---|---|---|---|---|---|---|---|---|
| | TST | CVT | CVT/ZCT | CVT/SCT | TST | CVT | CVT/ZCT | CVT/SCT | TST | CVT | CVT/ZCT | CVT/SCT |
| 400 | 6.18E9 | 4.03E9 | 6.36E9 | 1.39E10 | 3.30E11 | 2.15E11 | 3.39E11 | 5.13E11 | 8.29E11 | 3.05E11 | 3.78E11 | 4.60E11 |
| 600 | 5.19E10 | 4.21E10 | 5.12E10 | 7.19E10 | 7.36E11 | 5.97E11 | 7.28E11 | 8.98E11 | 1.36E12 | 8.82E11 | 9.71E11 | 1.06E12 |
| 1000 | 4.42E11 | 4.18E11 | 4.47E11 | 5.04E11 | 2.17E12 | 2.05E12 | 2.20E12 | 2.38E12 | 3.14E12 | 2.13E12 | 2.21E12 | 2.28E12 |
| 1200 | 8.77E11 | 7.19E11 | 7.54E11 | 8.18E11 | 3.30E12 | 2.70E12 | 2.84E12 | 3.01E12 | 4.49E12 | 3.32E12 | 3.40E12 | 3.48E12 |
| 1400 | 1.53E12 | 1.29E12 | 1.33E12 | 1.42E12 | 4.77E12 | 4.01E12 | 4.16E12 | 4.33E12 | 6.20E12 | 4.85E12 | 4.94E12 | 5.02E12 |
| 1800 | 3.66E12 | 3.19E12 | 3.26E12 | 3.38E12 | 8.85E12 | 7.71E12 | 7.88E12 | 8.09E12 | 1.09E13 | 9.14E12 | 9.24E12 | 9.33E12 |
| 2400 | 9.47E12 | 8.51E12 | 8.62E12 | 8.79E12 | 1.84E13 | 1.65E13 | 1.67E13 | 1.70E13 | 2.14E13 | 1.67E13 | 1.68E13 | 1.69E13 |
| 3000 | 1.92E13 | 1.53E13 | 1.54E13 | 1.56E13 | 3.26E13 | 2.60E13 | 2.62E13 | 2.65E13 | 3.69E13 | 2.63E13 | 2.64E13 | 2.65E13 |

bohr at 400, 1000, 2000, and 3000 K, respectively. In addition, Table 4 shows that the tunneling and curvature effects are important at temperatures below 600 K. These quantum effects may be ignored in the investigation of the dynamical properties of this reaction at high temperature.

## 4 Conclusion

1. The potential-energy barrier calculated at the UMP-SAC4 level of theory is 0.80 kcal/mol and agrees approximately with the experimental one. The heat of reaction at the same theoretical level is −27.3 kcal/mol and is in better agreement with the experimental value.

2. The MEP is followed at the UMP2/6-311G** level by intrinsic reaction coordinate theory. The changes in the geometry along the MEP suggest that the concerted interaction region of both the $N_{(1)}$—$H_{(3)}$ bond breaking and the $H_{(3)}$—$O_{(4)}$ bond forming is about $s = -0.2$–$0.8$ $(amu)^{1/2}$bohr. The changes in the frequencies and coupling constants along the MEP show that mode 3 plays an important role in the course of the hydrogen abstraction reaction.

3. The VTST rate constants calculated at the UQ-CISD(T) and UMP-SAC4 levels of theory are in good agreement with the values of Miller and Bowmann over the temperature range 700–3000 K and with the values of Dean et al. over the temperature range 400–800 K.

*Acknowledgement*. This work was supported by the National Natural Science Foundation of China.

## References

1. Miller JA, Bowman CT (1989) Prog Energy Combust Sci 15: 287
2. Dean AM, Hardy JE, Lyon RK (1982) 19th Symposium on International Combustion. The Combustion Institute, Pittsburgh, Pa. p 97
3. Truhlar DG, Garrett BC (1980) Acc Chem Res 13: 440
4. Garrett BC, Truhlar DG, Grev RS, Magnuson AW (1980) J Phys Chem 84: 1730
5. Truhlar DG, Isaacson AD, Garrett BC (1985) In: Baert (ed) Theory of chemical reaction dynamics. CRC Press, Boca Raton, p 65
6. Baldridge KM, Gordon MS, Steckler R, Truhlar DG (1989) J Phys Chem 93: 5107
7. Frisch MJ, Trucks GW, Head-Gordon M, Gill PMW, Wong MW, Foresman JB, Johnson BG, Schlegel HB, Robb MA, Replogle ES, Gomperts R, Andres JL, Raghavachari K, Binkley JS, Gonzalez C, Martin RL, Fox DJ, Defrees DJ, Stewart JJP, Pople JA (1992) Gaussian 92. Gaussian Pittsburgh, Pa
8. Hehre WJ, Radom L, Schleyer PvR, Pople JA (1986) Ab initio molecular orbital theory. Wiley, New York
9. Pople JA, Binkley JS, Seeger R (1976) Int J Quantum Chem Symp 10: 1
10. Pople JA, Head-Gordon M, Raghavachari K (1987) J Chem Phys 87: 5968
11. Gordon MS, Truhlar DG (1986) J Am Chem Soc 108: 5412
12. Truhlar DG, Kuppermann A (1971) J Am Chem Soc 93: 1840
13. Gonzalez C, Schlegel HB (1989) J Phys Chem 90: 2154
14. Gonzalez C, Schlegel HB (1990) J Phys Chem 94: 5523
15. Liu Y-P, Lynch GC, Truong TN, Lu D-h, Truhlar DG (1993) J Am Chem Soc 115: 2408
16. Steckler R, Chuang Y-Y, Fast PL, Corchado JC, Coitino EL, Hu W-P, Liu Y-P, Lynch GC, Nguyen K, Jackels CF, Gu MZ, Rossi I, Clayton S, Melissas V, Garrett BC, Isaacson AD, Truhlar DG (1997) POLYRATE version 7.4. University of Minnesota
17. Harmony MD, Schwendeman MD, Laurie VW, Kuczkowski RL, Schwendeman RH, Ramsay DA, Lovas FJ, Larfferty WJ, Maki AG (1979) J Phys. Chem Ref Data 8: 619
18. Jacox ME (1990) J Phys Chem Ref Data 19: 1387
19. Huber KP, Herzberg G (1979) Molecular spectra and molecular structure IV. Constants of diatomic molecules. Van Nostrand Reinhold, New York
20. Shimanouchi T (1977) J Phys Chem Ref Data 6: 993
21. Kerr JA, Parsonage MJ, Trotman-Dickenson AF (1974) In: Weast R (ed) Handbook of chemistry and physics, 55th edn. CRC Press, Boca Raton